Cellular biomechanics impairment in keratinocytes is associated with a C-terminal truncated desmoplakin: An atomic force microscopy investigation

Luca Puzzi[a,1], Daniele Borin[a,1], Valentina Martinelli[b], Luisa Mestroni[c], David P. Kelsell[d], Orfeo Sbaizero[a,*]

[a] Department of Engineering and Architecture, University of Trieste, Piazzale Europa 1, 34127 Trieste, Italy
[b] Molecular Medicine, International Center for Genetic Engineering and Biotechnology, Padriciano 99, 34149 Trieste, Italy
[c] Cardiovascular Institute & Adult Medical Genetics, University of Colorado Denver Anschutz Medical Campus, 12700 E. 19th Avenue, 80045 Aurora, CO, United States
[d] Blizard Institute, Barts and The London School of Medicine and Dentistry, Queen Mary University of London, Turner Street, Whitechapel, E1 2AD London, United Kingdom

ARTICLE INFO

Keywords:
Desmoplakin
Keratinocytes
Cellular biomechanics
Atomic force microscopy
Desmosome
Cytoplasmic architecture

ABSTRACT

In a tissue continuously challenged by mechanical stresses, such as the skin or the heart, cells perceive information about their microenvironment through several adhesive protein complexes and activate cell-signaling events to maintain tissue cohesion. Consequently, alteration of cell adhesion components leads to aberrant assembly of the associated cytoplasmic scaffolding and signaling pathways, which may reflect changes to the tissue physiology and mechanical resistance. Desmoplakin is an essential component of the cell–cell junction, anchoring the desmosomal protein complex to the intermediate filaments (IFs). Inherited mutations in desmoplakin are associated with both heart and skin disease (cardiocutaneous syndrome). In this study, we investigated the mechanical properties of human keratinocytes harboring a cardiocutaneous-associated homozygous C-terminal truncation in desmoplakin (JD-1) compared to a control keratinocyte line (K1). Using Single Cell Force Spectroscopy (SCFS) AFM-based measurements, JD-1 keratinocytes displayed an overall alteration in morphology, elasticity, adhesion capabilities and viscoelastic properties, highlighting the profound interconnection between the adhesome pathways and the IF scaffold.

1. Introduction

Skin homeostasis relies on a highly integrated network of proteins mediating cell adhesion and communication, thus facilitating cellular responses to the mechanical changes in their environment. In part, this is achieved via both cadherin and integrin interactions with actin microfilaments, microtubules and intermediate filaments (IFs). Specifically, IFs are mainly implicated in tissue strength, being able to resist to a high degree of deformation in association with desmosomes (Janmey et al., 1991; Suresh, 2007). Any perturbation of the desmosome/IF complex compromises tissue integrity, resulting in a pathological condition and demonstrating the importance of the desmosome/IF scaffolding (Bouvard et al., 2001; Fuchs and Cleveland, 1998; McMillan and Shimizu, 2001; Omary, 2009; Steinert and Bale, 1993). Desmoplakin (DSP) is a fundamental component of the intracellular desmosome structure, and it is abundantly expressed both in myocardial and epidermal tissues. DSP uses its COOH-terminal plakin repeat domain to anchor the IFs, including desmin (heart) and keratins (skin) (Kouklis et al., 1994; Meng et al., 1997; Stappenbeck and Green, 1992), while its N-terminus binds the armadillo proteins (plakoglobin and plakophilin) of the outer dense plaque, thus representing the final connection of the desmosome with the cytoskeleton. Mutations in the gene coding for DSP can be associated with a cardiocutaneous syndrome, including arrhythmogenic cardiomyopathy (ACM) and the skin disease palmoplantar keratoderma (PPK) (Norgett et al., 2000; Rampazzo et al., 2002). In this paper, we applied the Atomic Force Microscopy (AFM) technique to investigate the global biomechanical behavior of keratinocytes derived from the skin biopsy of a patient harboring a recessive cardiocutaneous associated desmoplakin mutation (termed JD-1). This mutation results in a protein with the C-terminus truncated and substituted by a sequence of eighteen amino-acids, which are not expressed in the wild type DSP, hampering its proper interaction with the IFs (Huen et al., 2002; Norgett et al., 2000). We found that loss of this C-terminal domain of DSP alters the biomechanical parameters of keratinocytes, including cellular adhesion, in agreement with data already published both *in vitro* (Huen et al., 2002) and *in vivo* (Norgett et al.,

* Corresponding author.
E-mail address: sbaizero@units.it (O. Sbaizero).
[1] These authors contributed equally to this work.

2000). Moreover, we detected modifications in the cellular viscoelastic response, highlighting the compromised status of the cytoskeletal architecture.

2. Materials and methods

2.1. Cell culture

After gaining both verbal and written consent, skin biopsies had been taken from both a cardiocutaneous patient harboring a homozygous recessive C-terminal mutation in DSP (JD-1) and from an unrelated control donor (K1), as described previously (Huen et al., 2002; Norgett et al., 2000). The complete aminoacidic sequences for mutant and control DSP are reported as Supplementary Information, whereas Western blot analysis showing the effect of truncation is provided in the work of Norgett et al. (2000). Ethical approval was obtained from the East London and City Health Authority. Primary keratinocytes had been immortalized with HPV16 (E6/E7) and cultured according to a published protocol (Huen et al., 2002). Briefly, immortalized control (K1) and JD-1 keratinocytes were cultured in DMEM/Ham's F12 (3:1) medium supplemented with 10% FCS, 4 mM glutamine, 0.4 μg/ml hydrocortisone, 0.1 nM cholera toxin, 5 μg/ml insulin and 10 ng/ml EGF and kept in the incubator at 37 °C and at 5% of CO_2.

2.2. Immunofluorescence and nuclear morphology evaluation

1.5×10^5 cells were seeded over gelatin-coated coverslips (0.02% w/v in ddH_2O). The next day, keratinocytes were fixed in PBS containing 4% PFA for 20 min at room temperature and then aldehydes were quenched with 0.1 M glycine in PBS for 20 min at room temperature. Cells were permeabilized with 0.5% Triton X-100 for 20 min, blocked with 20% goat serum in PBS for 1 h at room temperature and incubated with a mouse monoclonal anti α-tubulin (T5168) antibody (Sigma-Aldrich) at 1:4000 dilution overnight at 4 °C. Cells were then washed 3 times for 10 min with PBS and 0.05% Tween 20 and finally incubated with Alexa Fluor 488-conjugated anti-mouse secondary antibodies (Invitrogen) in 20% goat serum in PBS for 45 − 60 min at room temperature. F-actin filaments were counterstained with Alexa Fluor 594 Phalloidin (Life Technologies) at 1:500 dilution in PBS for 45 min at room temperature. Each slide was then mounted in Vectashield with DAPI (Vector Labs). For image acquisition, a Nikon A1$^+$ Confocal Microscope System was used with a Plan-Apochromat λ 60X/1.40 oil objective. Within each experiment, instrument settings were kept constant. All the relative acquired pictures are representative from at least three independent cell preparations. Nuclear area and circularity (defined as $4\pi Area/Perimeter^2$) of a total number of 78 JD-1 and 85 control keratinocytes, coming from 10 and 9 different optical frames respectively, were evaluated using ImageJ software.

2.3. Atomic force microscopy (AFM)

An AFM Solver Pro-M (NT-MDT, Moscow, Russia) was used to acquire cell morphology as well as force-displacement curves as previously described (Borin et al., 2017; Codan et al., 2014; Lanzicher et al., 2015). Briefly, a gold coated triangular cantilever modified with a gold microsphere with a diameter around 5 μm (sQUBE, Germany) was used to precisely apply a compression force on the nuclear portion of single cells, thus avoiding artefacts from substrate stiffness. The AFM analyses were performed directly on the Petri dishes at physiological conditions of medium and temperature. The day before the analysis, 1.5×10^5 cells were seeded on each dish and allowed to adhere for 24 h. The spring constant of the cantilever was measured with Sader's method and compared to that indicated by the supplier (0.08 N/m). To calibrate the cantilever deflection signal as necessary to process the collected data, curves of force versus the piezo-displacement were acquired on plastic substrate. The measured cells were selected at random as long as they had a healthy morphology and they were well spread. Preliminary scans were performed to define the nuclear position and the cell height. As the AFM tests are rate-dependent, and to avoid the influence of hydrodynamic forces, all experiments were performed at the same speed (1 μm/s) (Lu et al., 2006; Mathur et al., 2001). The total duration of examinations on a single Petri dish was never longer than 60 min to avoid major variations in the physiological parameters of the investigated cells.

2.4. Cell height, modeling cells elasticity and work of adhesion

Cell height measurements are determined by the AFM piezo displacement along the Z-axis. Briefly, after an AFM scan of a 100 μm per 100 μm field, each cell within this area was subjected to three consecutive indentations over the nucleus, at the same position. A second scan was then performed on the same area and the heights of each cell were measured and compared with the values of the first scan using Gwyddion software (gwyddion.net).

Cell elasticity was calculated applying the Sneddon's modification of the Hertz contact theory to the AFM force indentation curves; this model is satisfactory and conventionally used to yield a general idea of cell elasticity by the estimation of the Young's modulus (Carl and Schillers, 2008). The Hertz-Sneddon model for spherical tips has the form:

$$F = \frac{E}{(1-\nu^2)} \cdot \left(\frac{R_{sphere}^2 + a^2}{2} \cdot log \frac{R_{sphere} + a}{R_{sphere} - a} - aR_{sphere} \right) \quad (1)$$

$$\delta = \frac{a}{2} \cdot log \frac{R_{sphere} + a}{R_{sphere} - a} \quad (2)$$

where F is the loading force, E is the Young's modulus, υ the Poisson ratio (set to 0.5, assuming cell's incompressibility), R_{sphere} the sphere radius, a is the tip contact surface radius (function of the tip radius and penetration) and δ is the probe penetration into the cell. The loading force curves were processed through the AtomicJ software (Hermanowicz et al., 2014) fitting only the first μm of indentation.

The work of adhesion was evaluated by integrating the area under the plateau of the unloading curve, thus measuring the non-specific interaction of the gold probe with the cell membrane (Fig. 1A – black dotted box). For both Young's modulus and adhesion work evaluation, each cell was subjected to three consecutive indentations at the same position and the mean of the results was considered as a single cell value.

2.5. Cell viscoelasticity

Single cell force spectroscopy (SCFS) measurements were used to assess cell viscoelastic behavior by both plasticity index and stress-relaxation experiments. The viscoelastic parameter describing cell adaptability towards an external force, namely the plasticity index (ζ), was determined by subtracting the ratio between areas under loading (A_1) and unloading (A_2) curves along the y-axis to the value 1 (Klymenko et al., 2009) (Fig. 1A − red dotted box).

$$\zeta = 1 - (A_2/A_1) \quad (3)$$

Intermediate values between a fully elastic (ζ = 0) and a fully plastic behavior (ζ = 1), indicate mixed viscoelastic properties. As described previously, each cell was subjected to three consecutive indentations at the same position and the mean of the results was considered as a single cell value.

Stress relaxation tests were performed to assess the cell viscoelasticity under prolonged load in the so-called constant height mode (Moreno-Flores et al., 2010). A preliminary AFM scan was performed to characterize the investigated cells in terms of their height. Experimental procedures were divided into three time-intervals (Fig. 1B). Initially,

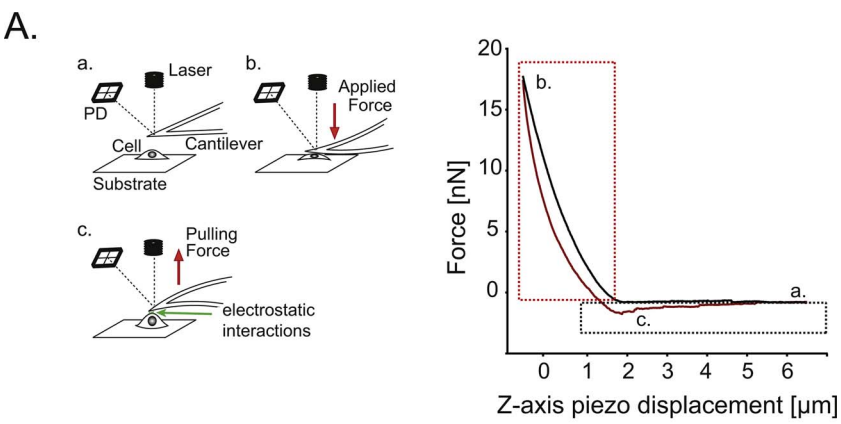

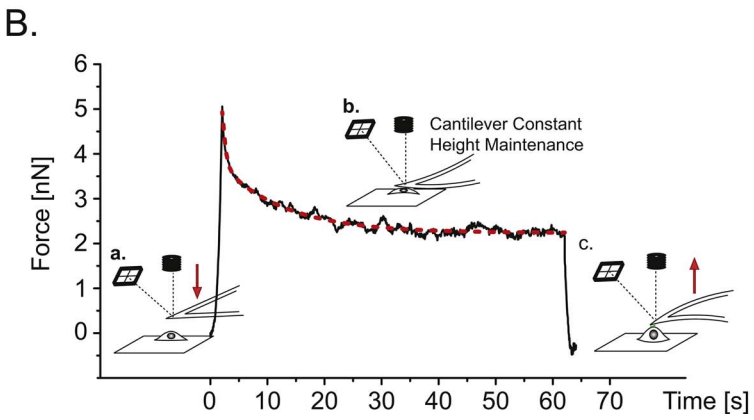

Fig. 1. Representation of an atomic force microscopy experiment. (A) Graphical explanation of an AFM experiment. The tip of the cantilever is positioned over the cell of interest (a.), moved along the Z-axis to indent the sample in the nuclear portion (b.) and then retracted (c.); the cantilever deflection is detected by a photodiode (PD). Plasticity index and work of adhesion were obtained by integrating the area between the approach and withdrawal curves, and are shown in the red and black dotted boxes, respectively. (B) Representative curve of a stress relaxation test performed on the nuclear region of cells. The tip of the cantilever approached the cell and indented it to 40% of its initial height (a.). The cantilever was maintained at the same height for a dwell period of 60 s (b.) and then retracted (c.). The dashed red line represents the bi-exponential fitting of the stress relaxation segment. (For interpretation of the references to color in this figure legend, the reader is referred to the web version of this article.)

the AFM spherical tip approached the cell surface with a speed of 1 µm/s. The indentation depth for each cell was set to 40% of its initial height and the movement of the piezo scanner in the Z direction was corrected with the deflection of the cantilever during cell compression. In the middle time interval, the cantilever base position was kept constant for a fixed time of 60 s, enough to reach a plateau in the relaxation profile, while the cantilever force was recorded with time. In the last time interval, the AFM tip was fully retracted from the cell. Force data relative to the relaxation phase were normalized (with the minimum force before indentation corresponding to 0 and the maximum force at the end of indentation corresponding to 1) and fitted with a bi-exponential curve with an offset according to the generalized Maxwell viscoelastic model, as follows:

$$G(t) = G_e + G_1 e^{\left(-t/\tau_1\right)} + G_2 e^{\left(-t/\tau_2\right)} \quad (4)$$

where G(t) is the normalized force profile and τ_1 and τ_2 are the two characteristic relaxation times. This model was chosen because a single exponential equation did not describe properly the initial part of the relaxation curve, while the use of a tri-exponential one did not significantly improve the quality of the fitting. The normalized profile was also used to calculate the percent relaxation at the end of the applied stress:

$$\%relax = [1 - G(t = 60s)]*100 \quad (5)$$

Each result was representative of a single cell.

2.6. Statistics

Experimental AFM data were tested with both Origin Pro and GraphPad Prism software. All data were first subjected to Shapiro-Wilk normality test and then the unpaired *t*-test with Welch's correction for normal distributions or, alternatively, the Wilcoxon-Mann-Whitney test, both with a two-tailed P-value, were employed. Data in the text are reported as mean of values ± standard deviation and graphically presented as 10th and 90th percentile box plots.

3. Results

3.1. 1C-terminal truncated desmoplakin affects cell morphology

AFM cell loading-unloading curves contain information about the biomechanical responses of a cell to external mechanical stimuli, while the piezo displacement along the Z-axis allows also the precise measure of the cell height. Indeed, our AFM analysis showed that JD-1 keratinocytes are bigger along the Z-axis than K1 by almost 33% (5.54 ± 0.75 µm for JD-1 versus 3.75 ± 0.84 µm for control, $P < 0.0001$; Fig. 2A). Since it has been already demonstrated that the lack of desmoplakin-IF interconnection leads to a collapse of keratin network (Broussard et al., 2017; Huen et al., 2002; Norgett et al., 2000), the correlation between JD-1 truncation and F-actin and microtubules structure was investigated. According to confocal microscopy data, no evident networks disorganization was detected (Fig. 2B). Next, the nuclear area and circularity were calculated from confocal microscope images and it was observed that JD-1 nuclei cover a greater area than control keratinocytes by almost 66% (368.2 ± 180.9 µm^2 for JD-1 versus 221.4 ± 106.8 µm^2 for control, $P < 0.0001$) even if not demonstrating a meaningful shape difference (Fig. 2C).

3.2. C-terminal truncated desmoplakin affects cell elasticity, viscoelasticity and work of adhesion

Elasticity data (Fig. 3A) showed that the JD-1 keratinocytes display a softer cell compared to the control keratinocytes, indeed Young's modulus is reduced by 34% for the mutated form (1.09 ± 0.75 kPa for

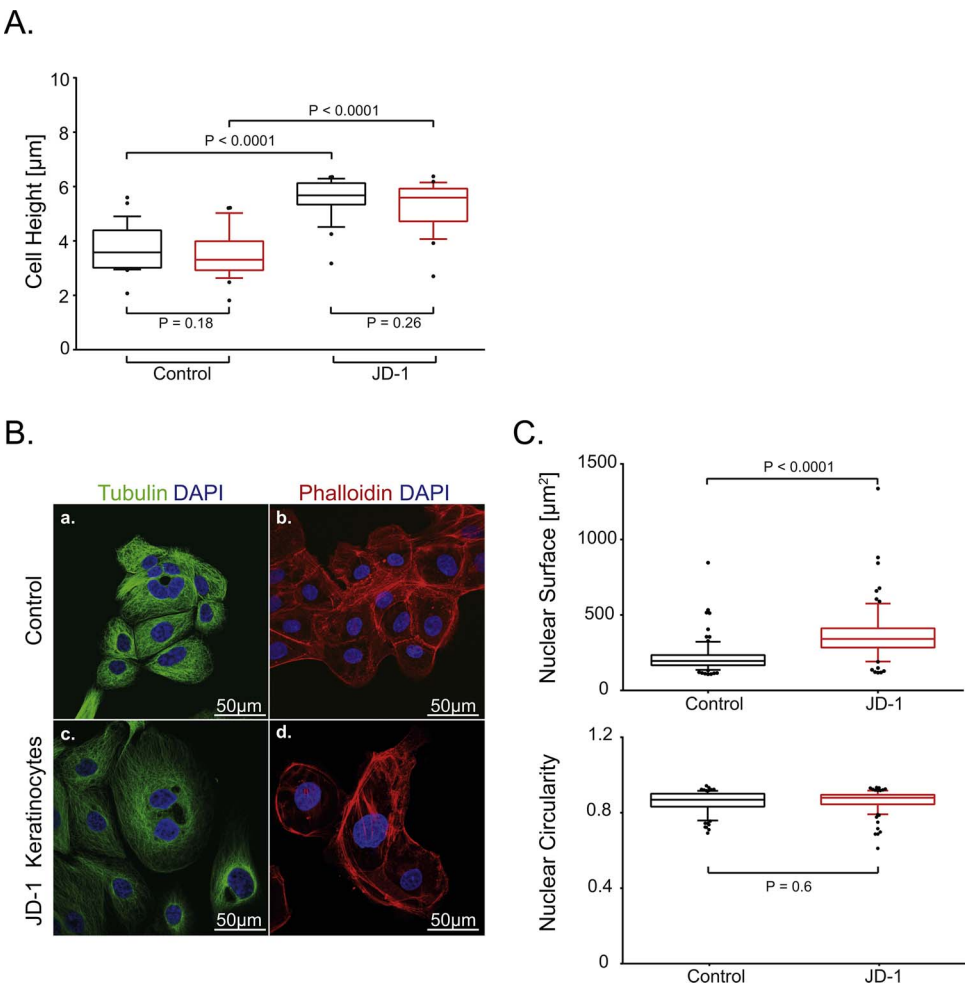

Fig. 2. C-terminal truncated desmoplakin affects cell morphology. (A) Measurements of the cell height through the AFM piezo displacement along the Z-axis before and after cell indentation are reported with black and red squared box plots, respectively. No statistically significant difference exists within each group before and after cell compression (3.75 ± 0.84 µm and 3.46 ± 0.81 µm, P = 0.18 for K1 and 5.54 ± 0.75 µm and 5.30 ± 0.86 µm, P = 0.26 for JD-1), whereas a difference was detected between the two groups (P < 0.0001), both before and after cell indentation. For this experiment, 28 cells for both K1 and JD-1 keratinocytes were examined, and measurements are reported as the mean ± standard deviation. (B) Representative pictures of confocal microscope analyses of microtubules (green, panels a. and c.) and actin microfilaments (red, panels b. and d.) were taken. The networks of both cytoplasmic components appear similar between JD-1 and K1 cells. Scale bar 50 µm. (C) Nuclear area (upper panel) and circularity (bottom panel) quantification analyses demonstrated increased nuclear size of JD-1 cells (221.4 ± 106.8 µm^2 for K1 versus 368.2 ± 180.9 µm^2 for JD-1; P < 0.0001), confirming our AFM data about cell height. A total number of 78 JD-1 and 85 K1 keratinocytes, coming from 10 and 9 different optical frames, respectively, were evaluated. Statistical analysis was performed using Shapiro-Wilk normality test and unpaired *t*-test with Welch's correction; the statistical significance is described by a two-tailed P value. (For interpretation of the references to color in this figure legend, the reader is referred to the web version of this article.)

JD-1 versus 1.63 ± 1.09 kPa for K1, P < 0.0001). At the same time, JD-1 keratinocytes are less viscous compared to control cells, and are able to store less energy in their cytoplasmic components if subjected to a not-prolonged mechanical stress, as shown by the plasticity index data displayed in Fig. 3 B (0.36 ± 0.08 for JD-1 versus 0.39 ± 0.10 for control, P = 0.03). These results could be associated with a lower

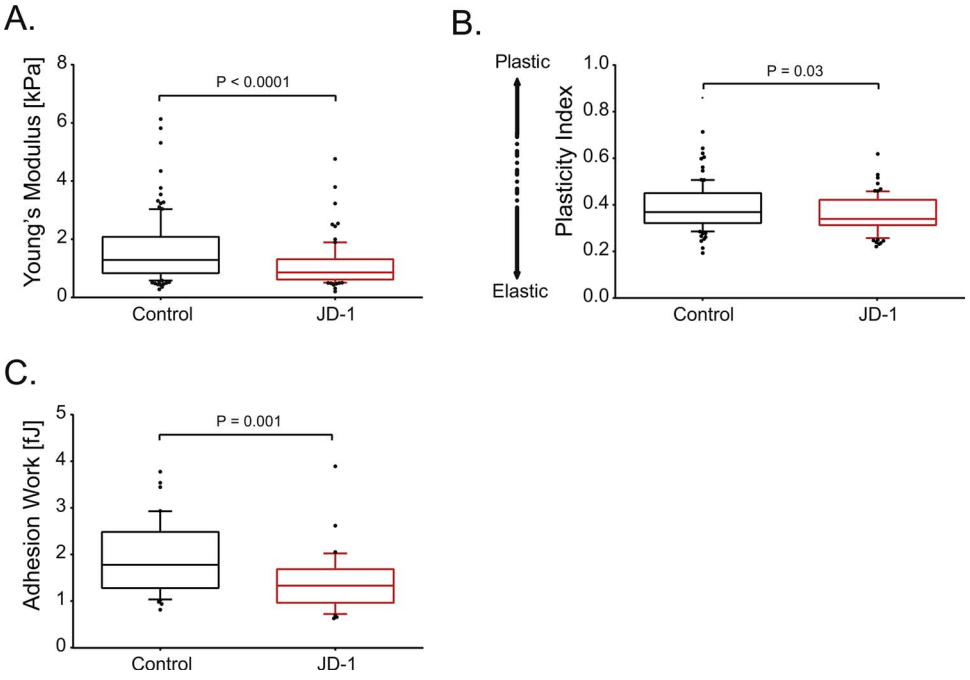

Fig. 3. C-terminal truncated desmoplakin alters cell elasticity, work of adhesion and plasticity index. (A) AFM analysis demonstrated that desmoplakin C-terminal modification affects whole cell elasticity, leading to a decrease of global cellular stiffness (1.63 ± 1.09 kPa n = 113 for K1 and 1.09 ± 0.75 kPa n = 81 for JD-1; P < 0.0001). (B) Viscoelasticity for short-term deformation, described by the plasticity index, was altered by DSP C-terminus truncation (0.39 ± 0.10 n = 90 for K1 and 0.36 ± 0.08 n = 78 for JD-1; P = 0.03). (C) A reduced work of adhesion was also observed in JD-1 cells (1.92 ± 0.76 fJ n = 45 for K1 and 1.41 ± 0.63 fJ n = 35 for JD-1; P = 0.001). Data are reported as the mean of all measurements ± standard deviation. Statistical analysis was performed using Shapiro-Wilk normality test and Wilcoxon-Mann-Whitney test; the statistical significance is described by a two-tailed P value. In all experiments, each cell was subjected to three consecutive indentations at the same position and the mean of the results was considered as a single cell value.

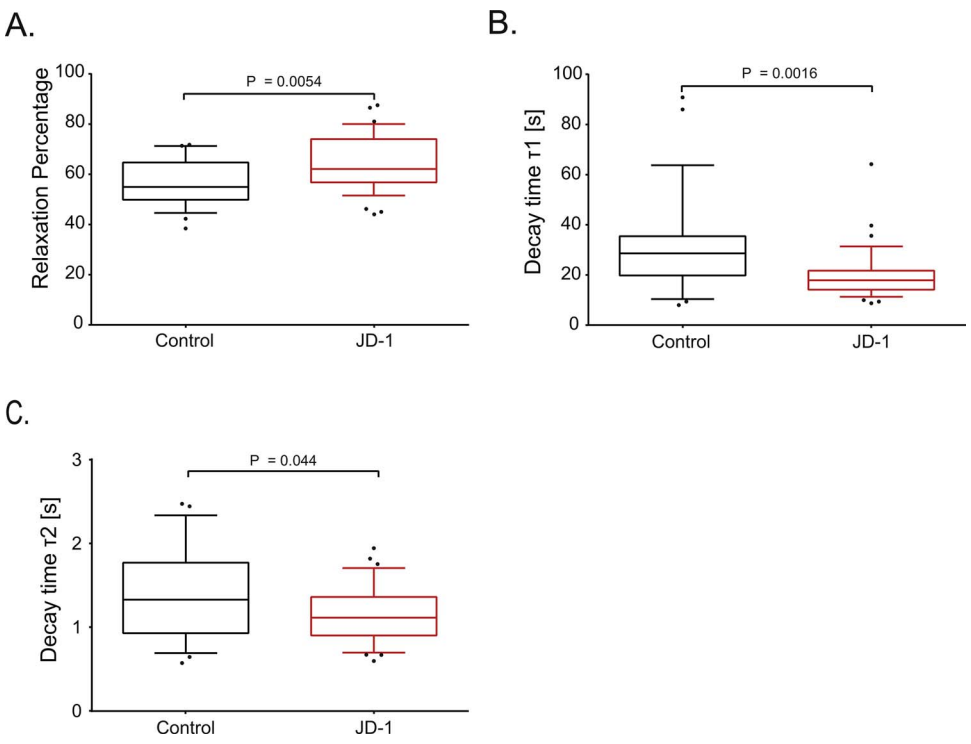

Fig. 4. C-terminal truncated desmoplakin influences long-term mechanical stress viscoelasticity. (A) Viscoelasticity comparison between control and JD-1 keratinocytes for long-term deformation assessed by stress-relaxation experiments indicates that C-terminal truncation of DSP affects the ability of cells to resist a prolonged mechanical load. Indeed, JD-1 viscoelasticity impairment is demonstrated by the calculated relaxation percentage (56.47 ± 9.14% for K1 versus 64.12 ± 10.91% for JD-1; P = 0.005). (B) Decay time τ1 (31.03 ± 19.9 s for K1 versus 20.13 ± 10.0 s for JD-1; P = 0.0016) is dramatically reduced. (**C**) Decay time τ2 is statistically different (1.40 ± 0.57 s for K1 versus 1.16 ± 0.34 s for JD-1; P = 0.044), also. A total number of 25 and 37 cells were employed for control and JD-1 keratinocytes, respectively. Data are reported as the mean of all measurements ± standard deviation. Statistical analysis was performed using Shapiro-Wilk normality test and unpaired *t*-test with Welch's correction or the Wilcoxon-Mann-Whitney test; the statistical significance is described by a two-tailed P value.

resistance to deformation due to a non-optimal transmission of mechanical stresses from the membrane to the inner part of the cell caused by desmoplakin-IF loss of contact, which in turn leads to keratin network remodeling (Lulevich et al., 2010; Ramms et al., 2013; Seltmann et al., 2013). The effect of the JD-1 mutation is also evident in the work of adhesion required to detach the sphere of the AFM cantilever from the cell membrane after indentation. As shown in Fig. 3C, adhesion work was lower for JD-1 compared to control of almost 25% (1.41 ± 0.63 fJ for JD-1 versus 1.92 ± 0.76 fJ for control, P = 0.001).

3.3. C-terminal truncated desmoplakin affects long-term stress relaxation

Next, to confirm plasticity index data, which allow analysis of the viscoelastic properties of cells after a short-term mechanical stress, long-term investigation was performed through stress relaxation experiments (Moreno-Flores et al., 2010). By fitting the stress-relaxation curves (Fig. 1B), the cellular relaxation times obtained highlighted a decreased viscoelasticity in JD-1 cells (τ1: 20.13 ± 10.0 s for JD-1 versus 31.03 ± 19.9 s for K1, P = 0.0016; τ2: 1.16 ± 0.34 s for JD-1 versus 1.40 ± 0.57 s for K1, P = 0.044, Fig. 4 B and 4C). Moreover, the analysis of percent relaxation confirmed a correlation between the correct cytoplasmic architecture (actin, tubulin and intermediate filaments) and the cellular resistance to prolonged mechanical stresses. Indeed, JD-1 keratinocytes relaxed more than control keratinocytes (64.12 ± 10.91% for JD-1 versus 56.47 ± 9.14% for K1, P = 0.005; Fig. 4A). Our data indicate that the lack of connection between desmoplakin and the intermediate filaments in the mutated cells has relevant effects both on the long-term (stress-relaxation) and in the short-term deformation (Young's modulus and plasticity index) that could be explained by the IF perturbations (Lulevich et al., 2010; Ramms et al., 2013; Seltmann et al., 2013), which in turn alter the overall viscoelasticity of the cell.

4. Discussion

This study highlighted the strict interconnection, from a biomechanical perspective, between adhesome components. The correct cytoskeletal architecture represents a pivotal feature in the conversion of mechanical stimuli into biochemical signals. In particular, IFs (as part of desmosomes) and Actin (as a component of the LINC − Linker of Nucleoskeleton and Cytoskeleton complex), are strongly integrated in convergent signaling pathways (Fournier et al., 2008; Martinez-Rico et al., 2010).

Desmoplakin in human keratinocytes is present in two splicing isoforms, DSPI and DSPII, both composed of three main domains (Fig. 5A). The N-terminal globular head, made of 1056 amino acids, binds the armadillo proteins (plakoglobin and plakophilins) in the intracellular portion of desmosome; the C-terminal globular tail is composed of 926 amino acids organized in three repeated plakin domains (A, B, C) which bind to the IFs. The central rod domain, which differs in length from DSPI (889 amino acids) and DSPII (290 amino acids), is responsible of DSP dimerization/oligomerization (Hudson et al., 2004).

In JD-1 keratinocytes, the C subdomain of the C-terminal tail is missing and replaced by a sequence of eighteen amino acids (Fig. 5C and Supplementary Information), which hampers the proper binding with IFs. In this scenario, the disconnection between desmoplakin and keratin in JD-1 cells dramatically affects both the mechano-transduction pathway and the cellular mechanics.

The approach used in this study, combining both loading-unloading and stress relaxation tests, allowed to investigate the mechanical properties of cells with short and long-term applied forces. Our data indicated that the alterations in the IFs network organization, as a consequence of the C-terminal truncated DSP (Huen et al., 2002; Norgett et al., 2000), is associated with a severe decrease of global elasticity (Young's modulus) and work of adhesion properties. In addition, it is responsible for the alteration of the cytoplasmic architecture which in turn exerts an effect on whole cell viscoelasticity.

Perturbation of the keratin IFs could also account for the loss of cytoskeletal network tensional equilibrium, which leads the cell to enlarge. Indeed, if we consider the cell as a sphere of radius R_{cell}, with a cell membrane of thickness h, its bending modulus κ, the in-plane shear modulus μ and the in-plane stretching modulus K, can be expressed as (Helfer et al., 2001):

$$\kappa = E\,h^3 / [12(1-\nu^2)] \quad (6)$$

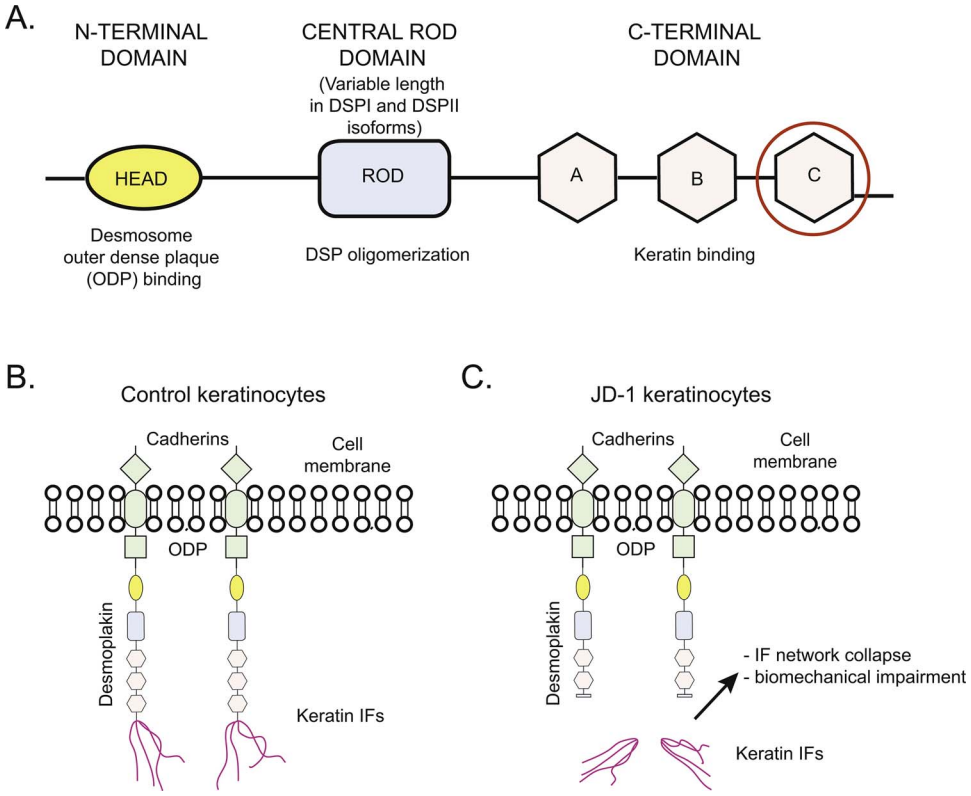

Fig. 5. Structure and function of desmoplakin in healthy and in JD-1 keratinocytes. (A) Representative cartoon showing the three domains of human wild-type DSP from healthy keratinocytes (K1), with their respective functions. (B) In healthy keratinocytes, DSP connects the cytoskeleton to the desmosome, binding the IFs through the C-terminal domain and the outer dense plaque (ODP) proteins plakoglobin and plakophilin, with the N-terminal head. (C) In JD-1 keratinocytes, the C subdomain (corresponding to C enclosed in the red circle in Fig. 5A) is substituted by a sequence of 18 amino acids, thus missing the link with IFs network. This results in the collapse of keratin network, hence impairing the biomechanics of the keratinocytes. (For interpretation of the references to color in this figure legend, the reader is referred to the web version of this article.)

$$\mu = E\,h/\,[2(1+\nu)] \quad (7)$$

$$K = E\,h\,/\,[2(1-\nu)] \quad (8)$$

where E is the Young's modulus (elasticity) and ν is the Poisson's ratio. Shear stress can be neglected since the lipids are in a “fluid” liquid crystalline state at physiological conditions (Daily et al., 1984; Helfer et al., 2001). During a radial expansion ξ the energies involved are therefore:

$$F_b \propto Eh^3\left(\frac{\xi}{R_{cell}{}^2}\right)^2 \quad \text{bending energy (9)}$$

$$F_s \propto Eh\left(\frac{\xi}{R_{cell}}\right)^2 \quad \text{stretching energy (10)}$$

In agreement with previous data (Huen et al., 2002; Norgett et al., 2000), our results underline that a change in the structure of desmosomes due to the disconnection of the keratin intermediate filaments to the face of desmosome also reduces the membrane stretching stiffness. Moreover, since both energies are a function of the elasticity, a lower Young’s modulus would indicate that a cell could increase its size using less energy, thus potentially explaining the increased dimensions of JD-1 cells compared to control keratinocytes.

5. Conclusions

Our study underlined that single cell force spectroscopy through AFM can be employed to describe biomechanical properties of living cells in which an altered intermediate filaments cytoskeletal architecture arise from desmoplakin genetic modification.

In the case of JD-1 keratinocytes, AFM data revealed that modification of desmoplakin, a protein connecting the intermediate filaments (IFs) to the desmosome plaque, induced a dramatic alteration of the tensional equilibrium of the cell, which in turn lead to a decreased cell stiffness (Young’s modulus), reduced adhesion work and cell enlargement.

Collectively, our results could be explained by the tensegrity model (Ingber, 2008), which explains how living cells maintain their shape being a pre-stressed structure, in which tensional forces are borne by actin and IFs, and these forces are balanced by microtubule filaments allowing the whole cellular structure to withstand a compression. Using this model, it has been demonstrated that when IFs are chemically disrupted, the cellular traction forces exerted on the extracellular matrix anchors decrease and the cell is more prone to deform (Eckes et al., 1998; Kolodney and Wysolmerski, 1992; Wang and Stamenovic, 2000). Similarly, DSP mutation may exert effects on the IFs network organization leading to a dramatic alteration of the mechanical properties respect to the control keratinocytes. As a future perspective of this work, atomic force microscopy could be used as a valuable tool to study the binding properties of the whole desmosomal cadherins in JD-1 cells.

6. Author contribution

This work was carried out in collaboration between all authors. DPK provided both JD-1 and control keratinocytes. LP and DB carried out AFM experiments and analyzed the data. LP and VM performed immunofluorescence analysis. LP carried out the statistical analysis. LP, DB, DPK and OS drafted the manuscript. All authors have contributed to, seen and approved the manuscript.

7. Funding

Financial support from the *Fondation Leducq*, Transatlantic Network of Excellence (14-CVD 03).

8. Competing of interest

The authors declare no competing or financial interests.

Acknowledgments

All the authors are sincerely grateful to Ilaria Pecorari for the useful suggestions about statistical treatment of experimental data. We would like to thank Dr. Sharon Graw for helpful manuscript revision.

Appendix A. Supplementary data

Supplementary data associated with this article can be found, in the online version, at https://doi.org/10.1016/j.micron.2017.12.005.

References

Borin, D., Puzzi, L., Martinelli, V., Cibinel, M., Lapasin, R., Sbaizero, O., 2017. An engineering insight into the relationship of selective cytoskeletal impairment and biomechanics of HeLa cells. Micron 102, 88–96.

Bouvard, D., Brakebusch, C., Gustafsson, E., Aszodi, A., Bengtsson, T., Berna, A., Fassler, R., 2001. Functional consequences of integrin gene mutations in mice. Circ. Res. 89, 211–223.

Broussard, J.A., Yang, R., Huang, C., Nathamgari, S.S.P., Beese, A.M., Godsel, L.M., Hegazy, M.H., Lee, S., Zhou, F., Sniadecki, N.J., Green, K.J., Espinosa, H.D., 2017. The desmoplakin/intermediate filament linkage regulates cell mechanics. Mol. Biol. Cell.

Carl, P., Schillers, H., 2008. Elasticity measurement of living cells with an atomic force microscope: data acquisition and processing. Pflugers Archiv. Eur. J. Physiol. 457, 551–559.

Codan, B., Del Favero, G., Martinelli, V., Long, C.S., Mestroni, L., Sbaizero, O., 2014. Exploring the elasticity and adhesion behavior of cardiac fibroblasts by atomic force microscopy indentation. Materials science & engineering. C. Mater. Biol. Appl. 40, 427–434.

Daily, B., Elson, E.L., Zahalak, G.I., 1984. Cell poking. Determination of the elastic area compressibility modulus of the erythrocyte membrane. Biophys. J . 45, 671–682.

Eckes, B., Dogic, D., Colucci-Guyon, E., Wang, N., Maniotis, A., Ingber, D., Merckling, A., Langa, F., Aumailley, M., Delouvee, A., Koteliansky, V., Babinet, C., Krieg, T., 1998. Impaired mechanical stability, migration and contractile capacity in vimentin-deficient fibroblasts. J. Cell Sci. 111 (Pt. 13), 1897–1907.

Fournier, A.K., Campbell, L.E., Castagnino, P., Liu, W.F., Chung, B.M., Weaver, V.M., Chen, C.S., Assoian, R.K., 2008. Rac-dependent cyclin D1 gene expression regulated by cadherin- and integrin-mediated adhesion. J. Cell Sci. 121, 226–233.

Fuchs, E., Cleveland, D.W., 1998. A structural scaffolding of intermediate filaments in health and disease. Science 279, 514–519.

Helfer, E., Harlepp, S., Bourdieu, L., Robert, J., MacKintosh, F.C., Chatenay, D., 2001. Buckling of actin-coated membranes under application of a local force. Phys. Rev. Lett. 87, 088103.

Hermanowicz, P., Sarna, M., Burda, K., Gabrys, H., 2014. AtomicJ: an open source software for analysis of force curves. Rev. Sci. Instrum. 85, 063703.

Hudson, T.Y., Fontao, L., Godsel, L.M., Choi, H., Huen, A.C., Borradori, L., Weis, W.I., Green, K.J., 2004. In vitro methods for investigating desmoplakin–intermediate filament interactions and their role in adhesive strength. In: In: Wilson, L., Tran, P. (Eds.), Methods in Cell Biology 78. Elsevier Inc., Cambridge, MA, USA, pp. 757–786.

Huen, A.C., Park, J.K., Godsel, L.M., Chen, X., Bannon, L.J., Amargo, E.V., Hudson, T.Y., Mongiu, A.K., Leigh, I.M., Kelsell, D.P., Gumbiner, B.M., Green, K.J., 2002. Intermediate filament-membrane attachments function synergistically with actin-dependent contacts to regulate intercellular adhesive strength. J. Cell Biol. 159, 1005–1017.

Ingber, D.E., 2008. Tensegrity and mechanotransduction. J. Bodyw. Mov. Ther. 12, 198–200.

Janmey, P.A., Euteneuer, U., Traub, P., Schliwa, M., 1991. Viscoelastic properties of vimentin compared with other filamentous biopolymer networks. J. Cell Biol. 113, 155–160.

Klymenko, O., Wiltowska-Zuber, J., Lekka, M., Kwiatek, W.M., 2009. Energy dissipation in the AFM elasticity measurements. Acta Phys. Pol., A 115, 548–551.

Kolodney, M.S., Wysolmerski, R.B., 1992. Isometric contraction by fibroblasts and endothelial cells in tissue culture: a quantitative study. J. Cell Biol. 117, 73–82.

Kouklis, P.D., Hutton, E., Fuchs, E., 1994. Making a connection: direct binding between keratin intermediate filaments and desmosomal proteins. J. Cell Biol. 127, 1049–1060.

Lanzicher, T., Martinelli, V., Puzzi, L., Del Favero, G., Codan, B., Long, C.S., Mestroni, L., Taylor, M.R., Sbaizero, O., 2015. The cardiomyopathy lamin A/C D192G mutation disrupts whole-cell biomechanics in cardiomyocytes as measured by atomic force microscopy loading-unloading curve analysis. Sci. Rep. 5, 13388.

Lu, Y.B., Franze, K., Seifert, G., Steinhauser, C., Kirchhoff, F., Wolburg, H., Guck, J., Janmey, P., Wei, E.Q., Kas, J., Reichenbach, A., 2006. Viscoelastic properties of individual glial cells and neurons in the CNS. Proc. Natl. Acad. Sci. U. S. A. 103, 17759–17764.

Lulevich, V., Yang, H.Y., Isseroff, R.R., Liu, G.Y., 2010. Single cell mechanics of keratinocyte cells. Ultramicroscopy 110, 1435–1442.

Martinez-Rico, C., Pincet, F., Thiery, J.P., Dufour, S., 2010. Integrins stimulate E-cadherin-mediated intercellular adhesion by regulating Src-kinase activation and actomyosin contractility. J. Cell Sci. 123, 712–722.

Mathur, A.B., Collinsworth, A.M., Reichert, W.M., Kraus, W.E., Truskey, G.A., 2001. Endothelial, cardiac muscle and skeletal muscle exhibit different viscous and elastic properties as determined by atomic force microscopy. J. Biomech. 34, 1545–1553.

McMillan, J.R., Shimizu, H., 2001. Desmosomes: structure and function in normal and diseased epidermis. J. Dermatol. 28, 291–298.

Meng, J.J., Bornslaeger, E.A., Green, K.J., Steinert, P.M., Ip, W., 1997. Two-hybrid analysis reveals fundamental differences in direct interactions between desmoplakin and cell type-specific intermediate filaments. J. Biol. Chem. 272, 21495–21503.

Moreno-Flores, S., Benitez, R., Vivanco, M.D., Toca-Herrera, J.L., 2010. Stress relaxation microscopy: imaging local stress in cells. J. Biomech. 43, 349–354.

Norgett, E.E., Hatsell, S.J., Carvajal-Huerta, L., Cabezas, J.C., Common, J., Purkis, P.E., Whittock, N., Leigh, I.M., Stevens, H.P., Kelsell, D.P., 2000. Recessive mutation in desmoplakin disrupts desmoplakin-intermediate filament interactions and causes dilated cardiomyopathy, woolly hair and keratoderma. Hum. Mol. Genet. 9, 2761–2766.

Omary, M.B., 2009. IF-pathies: a broad spectrum of intermediate filament-associated diseases. J. Clin. Invest. 119, 1756–1762.

Ramms, L., Fabris, G., Windoffer, R., Schwarz, N., Springer, R., Zhou, C., Lazar, J., Stiefel, S., Hersch, N., Schnakenberg, U., Magin, T.M., Leube, R.E., Merkel, R., Hoffmann, B., 2013. Keratins as the main component for the mechanical integrity of keratinocytes. Proc. Natl. Acad. Sci. U. S. A. 110, 18513–18518.

Rampazzo, A., Nava, A., Malacrida, S., Beffagna, G., Bauce, B., Rossi, V., Zimbello, R., Simionati, B., Basso, C., Thiene, G., Towbin, J.A., Danieli, G.A., 2002. Mutation in human desmoplakin domain binding to plakoglobin causes a dominant form of arrhythmogenic right ventricular cardiomyopathy. Am. J. Hum. Genet. 71, 1200–1206.

Seltmann, K., Fritsch, A.W., Kas, J.A., Magin, T.M., 2013. Keratins significantly contribute to cell stiffness and impact invasive behavior. Proc. Natl. Acad. Sci. U. S. A. 110, 18507–18512.

Stappenbeck, T.S., Green, K.J., 1992. The desmoplakin carboxyl terminus coaligns with and specifically disrupts intermediate filament networks when expressed in cultured cells. J. Cell Biol. 116, 1197–1209.

Steinert, P.M., Bale, S.J., 1993. Genetic skin diseases caused by mutations in keratin intermediate filaments. Trends in Genetics: TIG 9, 280–284.

Suresh, S., 2007. Biomechanics and biophysics of cancer cells. Acta Biomater. 3, 413–438.

Wang, N., Stamenovic, D., 2000. Contribution of intermediate filaments to cell stiffness, stiffening, and growth. Am. J. Physiol. Cell Physiol. 279, C188–194.